NONLINEAR PATTERNS IN URBAN CRIME - HOTSPOTS, BIFURCATIONS, AND SUPPRESSION*

M.B. SHORT†, A.L. BERTOZZI†, AND P.J. BRANTINGHAM‡

Abstract. We present a weakly nonlinear analysis of our recently developed model for the formation of crime patterns. Using a perturbative approach, we find amplitude equations that govern the development of crime "hotspot" patterns in our system in both the 1D and radially symmetric 2D cases. In addition to the supercritical spots already shown to exist in our previous work, we prove here the existence of subcritical hotspots that arise via a subcritical pitchfork bifurcation in 1D and a transcritical bifurcation in 2D. We present numerical results that both validate our analytical findings and confirm the existence of these subcritical hotspots in the non-radially symmetric 2D case. Finally, we examine the differences between these two types of hotspots with regard to attempted hotspot suppression, referencing the varying levels of success such attempts have had in real world scenarios.

Key words. bifurcations and instability, pattern formation, crime modeling

AMS subject classifications. 70K50, 70K60, 91D99

1. Introduction. The study of pattern formation in physical and mathematical systems has a long and interesting history. This general subject area is also quite diverse, examining biological (see, as a small sample, [32, 24, 23]), geological ([29, 10, 2]), and even sociological systems ([26, 13]), to name but a few. Though these various subjects and systems may seem completely unrelated, the mathematics describing the patterns in each are surprisingly similar. Consequently, a robust, powerful, and universal set of mathematical tools has been developed to study such systems, and the employment of these tools can lead to better understanding of pattern forming systems, regardless of their specific nature.

Recently, we set forth to develop a mathematical model to describe the spatio-temporal patterns of urban crime, specifically burglary [30]. Using well-known criminological ideas regarding the way in which criminal events effect future crime risk in a location, and the way in which risk can spread from one area to another [16, 17, 18, 1], we constructed a model consisting of two coupled, nonlinear partial differential equations that may describe the formation and dynamics of crime "hotspots" - spatio-temporal clusters of high crime. Using a simple linear stability analysis of our model, we found that the homogeneous system can be unstable to disturbances of specific wavenumbers under certain parameter regimes, leading to hotspot formation. However, our previous work stopped there, with no investigation of the possibility of hotspots outside of this linearly unstable regime. This paper addresses this possibility by performing a weakly-nonlinear analysis on our system and developing amplitude equations for the model. By investigating the possible bifurcations in the steady state solutions of our system both analytically and numerically, we indeed find that stable, "large" amplitude hotspots may exist even in the linearly stable regime.

The fact that these subcritical hotspots exist within our system is especially interesting when attempting to understand the outcome of hotspot suppression, typically by police executing a strategy known as hotspot policing, which has become dominant

*This work supported by NSF grant BCS-0527388, ARO MURI grant 50363-MA-MUR, and the Department of Defense.

†Department of Mathematics, UCLA, Los Angeles, CA 90095

‡Department of Anthropology, UCLA, Los Angeles, CA 90095

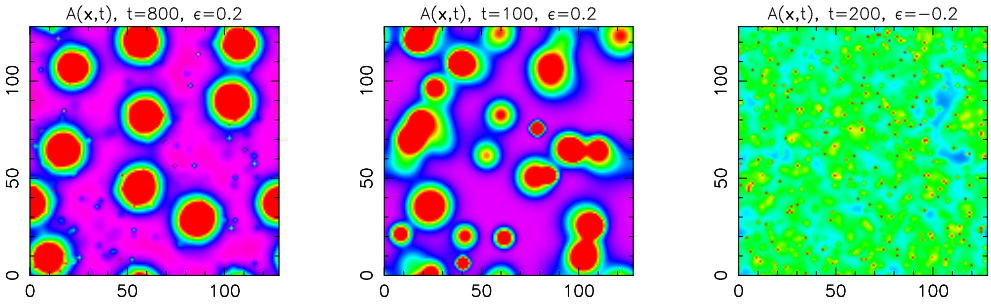

FIG. 2.1. *Example output from the discrete system. These colormaps display high A in red, $\overline{A}$ in green, and low A in blue to purple. In (a) is an example of stationary hotspots, in (b) is an example of transitory hotspots, and in (c) is an example of no hotspots.*

over the past two decades [6, 4, 5, 36, 35]. Recognizing that crime tends to form dense clusters in space and time, leaving some areas with little or no crime problem, police routinely target their limited resources at those locations experiencing high crime. That hotspot policing would be an improvement over random patrol is uncontroversial; it has been well-known since the 1970s that random patrol has little measurable effect on crime [20]. However, questions have been raised about whether hotspot policing leads to lasting hotspot reductions, or simply the displacement of hotspots from one area to another [25, 3, 7]. The present research provides a formal theoretical foundation for understanding different potential outcomes from hotspot policing, in relation to the classification of hotspots as either supercritical or subcritical.

The remainder of the paper is organized as follows. In Section 2, we give a brief introduction to our crime model and the major results found in [30]. In Section 3, we perform a weakly nonlinear analysis of our system in both the 1D and the radially symmetric 2D case, deriving some analytical results for the amplitude equations and bifurcations governing the hotspots exhibited by the system. In Section 4, we compare these analytical results to numerical solutions in the 1D and radially symmetric 2D case, as well as the fully 2D system. Finally, in Section 5, we explore the possible results of hotspot suppression qualitatively and numerically using both the continuum and discrete models.

2. Background. We being by reviewing the results of [30]. First, we developed an agent-based model of criminal activity that aims to reproduce the known phenomena of repeat and near-repeat victimization [16, 17, 18, 1], whereby crime risk becomes elevated in an area and its surroundings following an initial event there. The model couples the dynamics of moving, offending criminals on a 2D lattice with an underlying scalar field $A(\mathbf{x}, t)$ that we refer to as the attractiveness. As the name implies, the attractiveness field is a measure of how desirable any given location $\mathbf{x}$ is as a target for criminal activity, with the numerical value of the field giving the stochastic rate of offending for criminals at that location. When moving, criminals actively seek out areas of high A, and are more likely to commit crimes in those areas once they reach them. Upon commission of a crime, agents are removed from the system; agents are also added into the system at a set rate at each lattice point. Repeat and near-repeat victimization are incorporated by increasing the attractiveness at any location that is subject to a criminal event, and allowing that increased attractiveness to spread to

neighboring locations as time goes by. This increased attractiveness eventually decays back to a baseline value A^0 if no other events occur at that location. The model thus described contains a number of parameters, and depending upon the choice of these parameters, the system may exhibit three general types of behavior: stationary (fixed in space) crime hotspots, transitory (moving about in space or appearing and disappearing in time) hotspots, or no hotspots at all; these three cases are illustrated in Fig. 2.1.

We then developed a partial differential equation (PDE) model as a hydrodynamic limit of our continuum system, which is presented here in the dimensionless form

$$\frac{\partial A}{\partial t} = \eta \nabla^2 A - A + A^0 + \rho A \ , \tag{2.1}$$

$$\frac{\partial \rho}{\partial t} = \vec{\nabla} \left[\vec{\nabla} \rho - \frac{2\rho}{A} \vec{\nabla} A \right] - \rho A + \overline{A} - A^0 \ , \tag{2.2}$$

where ρ is the number density of criminal agents. In essence, crimes occur locally at rate ρA, and each such crime causes A to increase. In addition, A diffuses with dimensionless diffusion coefficient η (assumed less than 1), and decays exponentially to the baseline value A^0. Criminals exhibit diffusive motion with an advective bias up gradients of $\ln A$. Finally, criminals are subtracted from the system when they commit a crime, and are added back at a constant rate $\overline{A} - A^0$ [1]. These equations exhibit a general reaction-diffusion form, and are similar to models of chemotaxis such as the Keller-Segel model, which are well studied in the literature (see for example [19, 15, 34, 9, 12, 21, 31, 14, 8, 27]).

The continuum system described by Eqns. 2.1 and 2.2 may display two of the three behaviors from the discrete system - stationary hotspots or no hotspots. Transitory hotspots are not seen in the continuum approximation, as they are the result of statistical noise that is removed in the hydrodynamic limit. We showed that the formation of hotspots in this system may arise as a result of a linear instability toward perturbations of certain wavenumbers $\mathbf{k}$, and that the dispersion relation could be written as

$$\sigma(\mathbf{k}) = -\left[1 + \overline{A} - \overline{\rho} + |\mathbf{k}|^2(1+\eta)\right]/2 + \sqrt{\left[1 + \overline{A} - \overline{\rho} + |\mathbf{k}|^2(1+\eta)\right]^2/4 - \left(\eta|\mathbf{k}|^4 - (3\overline{\rho} - \eta\overline{A} - 1)|\mathbf{k}|^2 + \overline{A}\right)} \ , \tag{2.3}$$

where

$$\overline{\rho} = 1 - \frac{A^0}{\overline{A}} \ . \tag{2.4}$$

The instability criterion, therefore, could be written as

$$A^0 < A^0_* = \frac{2}{3}\overline{A} - \frac{1}{3}\eta\overline{A}^2 - \frac{2}{3}\overline{A}\sqrt{\eta\overline{A}} \ . \tag{2.5}$$

In other words, if the baseline attractiveness is less than some critical value A^0_*, the system will be linearly unstable (exhibit some modes with a positive σ). Finally, we

[1] The choice of the notation $\overline{A}$ here is due to the fact that, at steady state, this quantity is indeed the spatially averaged value of $A(\mathbf{x})$, regardless of the other parameters or whether hotspots are displayed or not.

showed that the maximally unstable mode $\mathbf{k}_{\max}$ is given by

$$|\mathbf{k}_{\max}|^2 = (1-\overline{A})/(1-\eta) - \overline{\rho}(5-\eta)/(1-\eta)^2 + \sqrt{\eta(1+\eta)^2\overline{\rho}\left[\left(\overline{A}(3-\eta)-2\right)(1-\eta)+2\overline{\rho}(3-\eta)\right]}/\eta(1-\eta)^2 \ . \quad (2.6)$$

Note for future reference that, when $A^0 = A^0_*$, the maximally growing mode can be greatly simplified to

$$|\mathbf{k}_{\max}|^2 \equiv |\mathbf{k}_*|^2 = \sqrt{\frac{\overline{A}}{\eta}} \ . \quad (2.7)$$

3. Weakly nonlinear analysis. Our goal now is to more deeply examine the continuum system of Eqns. 2.1 and 2.2 and to move beyond a simple linear stability analysis, the results of which are shown above. We will accomplish this by means of a weakly nonlinear analysis, using a standard perturbative expansion approach to derive amplitude equations for our system [11, 33].

We begin by considering a parameter regime such that our system is only slightly linearly unstable (or stable). Mathematically, we define a small parameter ϵ via the equation

$$A^0 = A^0_* - \epsilon\overline{A} \ , \quad (3.1)$$

where our system will therefore be unstable for positive ϵ, and stable for negative ϵ. The choice of scaling in the above equation gives firm upper and lower limits for the possible values of ϵ. At the high end, we have an $\epsilon_{\max}$ where $A^0 = 0$; at the low end, we have a negative $\epsilon_{\min}$ where $A^0 = \overline{A}$. These two values are given by:

$$\epsilon_{\max} = \frac{2}{3} - \frac{1}{3}\eta\overline{A} - \frac{2}{3}\sqrt{\eta\overline{A}} \ , \quad (3.2)$$

$$\epsilon_{\min} = -\frac{1}{3} - \frac{1}{3}\eta\overline{A} - \frac{2}{3}\sqrt{\eta\overline{A}} \ . \quad (3.3)$$

Note that the difference between these is always 1.

Returning again to the results of the linear stability analysis, when we substitute Eq. 3.1 into Eq. 2.3 and expand for small ϵ, we find that the growth rate for the $\mathbf{k}_*$ mode is given by

$$\sigma(\mathbf{k}_*) = \sigma_*\epsilon + O(\epsilon^2) \ , \quad (3.4)$$

where

$$\sigma_* = \frac{9\eta|\mathbf{k}_*|^2}{(1+\eta|\mathbf{k}_*|^2)\left[2\eta+\eta|\mathbf{k}_*|^2(3-\eta)\right]} \ . \quad (3.5)$$

Using this result, we see that we can define a new slow time variable $T = |\epsilon|t$ that describes the dynamics of the system when near the stability transition; this means that the ∂_t in Eqns. 2.1 and 2.2 becomes $|\epsilon|\partial_T$. We use $|\epsilon|$ here to make our future results valid regardless of the sign of ϵ, though this means that we must rewrite Eq. 3.1 as

$$A^0 = A^0_* - \text{sign}(\epsilon)|\epsilon|\overline{A} \ . \quad (3.6)$$

At this point, Eqns. 2.1 and 2.2 can be rewritten as

$$|\epsilon|\frac{\partial A}{\partial T} = \eta|\mathbf{k}_*|^2\nabla^2 A - A + A_*^0 - \text{sign}(\epsilon)\eta|\mathbf{k}_*|^4|\epsilon| + \rho A \ , \tag{3.7}$$

$$|\epsilon|\frac{\partial \rho}{\partial T} = |\mathbf{k}_*|^2\vec{\nabla}\left[\vec{\nabla}\rho - \frac{2\rho}{A}\vec{\nabla}A\right] - \rho A + \eta|\mathbf{k}_*|^4 - A_*^0 + \text{sign}(\epsilon)\eta|\mathbf{k}_*|^4|\epsilon| \ . \tag{3.8}$$

Note that we have defined a new spatial variable $\tilde{x} \equiv |\mathbf{k}_*|x$ here, but that we will continue to refer to $\tilde{x}$ as x in the future.

Next, we express A and ρ as expansions in our small parameter of the form:

$$A(\mathbf{x},T) = \overline{A} + \sum_{i=1}^{\infty}|\epsilon|^{\alpha_D i}A^{(i)}(\mathbf{x},T) \ , \tag{3.9}$$

$$\rho(\mathbf{x},T) = 1 - \frac{A_*^0}{\overline{A}} + \sum_{i=1}^{\infty}|\epsilon|^{\alpha_D i}\rho^{(i)}(\mathbf{x},T) \ , \tag{3.10}$$

where α_D is a rational number that will depend on the number of spatial dimensions we are interested in. We substitute these expansions into our differential equations and then separate the resulting equations by powers of $|\epsilon|$. We note that upon doing this, Eq. 3.7 can be used to simply solve for a given $\rho^{(i)}(\mathbf{x},T)$ algebraically in terms of lower order $\rho^{(j)}(\mathbf{x},T)$ and $A^{(j)}(\mathbf{x},T)$ and their derivatives, and that this result can then be substituted into Eq. 3.8. This leaves a series of fourth order differential equations to be solved that involve only the various $A^{(i)}(\mathbf{x},T)$, each of which is of the form

$$(\nabla^2+1)^2A^{(i)}(\mathbf{x},T) = f_i\left[A^{(1)}(\mathbf{x},T)\right] \ , \tag{3.11}$$

where f_i is a possibly nonlinear function.

3.1. 1D. For one dimension $\alpha_D = 1/2$, so the first interesting equation occurs at order $|\epsilon|^{1/2}$. This equation is simply

$$(\nabla^2+1)^2A^{(1)}(x,T) = 0 \ . \tag{3.12}$$

Let us now restrict our solution to a domain $x \in [0,L]$ where $L = 2n\pi$ for some integer $n > 0$, and impose periodic boundary conditions for both $A(x,T)$ and $\rho(x,T)$. The solution to Eq. 3.12 for these boundary conditions is simply

$$A^{(1)}(x,T) = P(T)e^{ix} + \text{c.c.} \ , \tag{3.13}$$

where $P(T)$ is the amplitude that at this point is simply an integration constant and "c.c." denotes the complex conjugate.

At order $|\epsilon|$, we find the equation

$$\left(\nabla^2+1\right)^2A^{(2)}(x,T) = \frac{4\left(1-\eta^2k_*^4\right)}{\eta^2k_*^6}\left[P(T)^2e^{2ix} + \text{c.c.}\right] \ . \tag{3.14}$$

The particular solution to this equation, which is all we are after, is

$$A^{(2)}(x,T) = \frac{4\left(1-\eta^2k_*^4\right)}{9\eta^2k_*^6}\left[P(T)^2e^{2ix} + \text{c.c.}\right] \ . \tag{3.15}$$

At order $|\epsilon|^{3/2}$, we find the equation

$$\left(\nabla^2+1\right)^2 A^{(3)}(x,T) = f_{3,1}\left[P(T);\eta,k_*\right]e^{ix} + f_{3,3}\left[P(T);\eta,k_*\right]e^{3ix} + \text{c.c.}\ ; \quad (3.16)$$

we do not reproduce the full expressions for $f_{3,i}$ here for sake of simplicity. The particular solution to this equation is

$$A^{(3)}(x,T) = -\frac{f_{3,1}\left[P(T);\eta,k_*\right]}{8}x^2e^{ix} + \frac{f_{3,3}\left[P(T);\eta,k_*\right]}{64}e^{3ix} + \text{c.c.}\ . \quad (3.17)$$

Note that this solution contains a term of the form x^2e^{ix} due to the secular e^{ix} term in Eq. 3.16. This secular solution term, and those found at higher orders in ϵ, will give our amplitude equation in the end, as all of these terms must vanish in order for the solution to fit the boundary conditions. If we simply desire the amplitude equation to the current order in ϵ, then, we must enforce that $f_{3,1}\left[P(T);\eta,k_*\right]=0$. Upon doing this, rescaling T back to t and letting $|\epsilon|^{1/2}P(t)\equiv Q(t)$, we find the amplitude equation

$$Q_t = \sigma_*\epsilon Q - C_1(\eta,k_*)|Q|^2Q\ , \quad (3.18)$$

where

$$C_1(\eta,k_*) = \frac{-8+56\eta k_*^2-31\eta^2k_*^4-8\eta^3k_*^6}{3\eta^2k_*^8\left[2\eta+\eta k_*^2(3-\eta)\right]}\ , \quad (3.19)$$

and σ_* is given by Eq. 3.5 above. This is the standard form for a dynamical system exhibiting a pitchfork bifurcation, with the distinction between a supercritical and subcritical bifurcation determined by the sign of C_1. Upon inspection, it is found that C_1 will be negative for any $\eta k_*^2<0.157$ (indicating a subcritical pitchfork bifurcation here) and positive otherwise (indicating a supercritical pitchfork bifurcation). The steady state value Q_s is either zero (the homogeneous case) or given by

$$Q_s = \pm\sqrt{\frac{\sigma_*\epsilon}{c_1(\eta,k_*)}}\ . \quad (3.20)$$

Finally, our solution for Q is only valid to order $|\epsilon|$, so our solution for $A(x,T)$ is also only valid to this order, and is given by

$$A(x,t) = \overline{A} + Q(t)e^{ix} + \frac{4\left(1-\eta^2k_*^4\right)}{9\eta^2k_*^6}Q(t)^2e^{2ix} + \text{c.c}\ . \quad (3.21)$$

One can in general continue the expansion up to higher orders in ϵ by defining subsequent slow timescales T_i for $i\geq 2$, each of which will modify ∂_t by adding a term $|\epsilon|^i\partial_{T_i}$. One then continues with the above results and eliminates the secular solutions at higher orders in the expansion, with the net result being amplitude equations that govern the various P_{T_i}. In practice, though, the algebra up to that point is quite expansive and little is gained by giving the exact expressions found. However, using a symbolic computing platform such as *Mathematica*, one can compute higher order solutions relatively quickly and easily; we will show the results of this when we discuss numerical results later.

3.2. 2D, radially symmetric. In this regime, $\alpha_D = 1$, so the first interesting equation in our system is proportional to $|\epsilon|$ and is

$$\left(\nabla^2 + 1\right)^2 A^{(1)}(r,T) = 0 \ . \tag{3.22}$$

Of course, the Laplacian operator in this case is different than that in 1D, as is the domain of the solutions. We now consider solutions on a disk $r \in [0, R]$ with $R = \alpha_{1,n}$, where $\alpha_{1,n}$ is the n^{th} root of the Bessel function $J_1(r)$; we enforce Neumann conditions on the boundary edge. For these boundary conditions, the solution at this order is

$$A^{(1)}(r,T) = P(T)J_0(r) \ . \tag{3.23}$$

At the next order, we find an equation for $A^{(2)}(r,T)$ that is

$$\begin{aligned}\left(\nabla^2 + 1\right)^2 A^{(2)}(r,T) = \\ \frac{9\eta k_*^2 P(T)\text{sign}(\epsilon) - \left(1+\eta k_*^2\right)\left[2\eta + \eta k_*^2(3-\eta)\right] P_T(T)}{3\eta^2 k_*^4} J_0(r) + \\ \frac{2\left(1-\eta^2 k_*^4\right)}{\eta^2 k_*^6} P(T)^2 \left[J_0^2(r) - J_1^2(r)\right] \ .\end{aligned} \tag{3.24}$$

Now, as before, we will need to eliminate any secular term proportional to $J_0(r)$ on the right hand side of this equation so that our solution will respect the boundary conditions imposed. In order to do so, we take advantage of the fact that the Bessel functions can be used as an orthogonal basis for expanding other functions, so we are free to write the $J_0^2(r) - J_1^2(r)$ portion on the right as a sum of Bessel functions to the first power, one of which will be $J_0(r)$. With the definition that

$$q = \frac{2\displaystyle\int_0^R r J_0(r)\left[J_0^2(r) - J_1^2(r)\right] dr}{R^2 J_0^2(R)} \ , \tag{3.25}$$

we see that setting the secular term to zero (and rescaling T to t and letting $|\epsilon|P(t) \equiv Q(t)$) is equivalent to the equation

$$Q_t = \sigma_* \epsilon Q + C_2(\eta, k_*) Q^2 \ , \tag{3.26}$$

where

$$C_2(\eta, k_*) = \frac{6q(1-\eta^2 k_*^4)}{k_*^2\left(1+\eta k_*^2\right)\left[2\eta + \eta k_*^2(3-\eta)\right]} \ . \tag{3.27}$$

Hence, we find that in the 2D, radially symmetric case our system will undergo a transcritical bifurcation. Interestingly, the constant C_2 will always be positive for any value of ηk_*^2 for which the above analysis is valid. That is, C_2 would only be negative if $\eta k_*^2 > 1$, but the maximum value of ηk_*^2 for which linear instability is at all possible (which must be the case for our analysis to work) is $\eta k_*^2 = \sqrt{3} - 1 < 1$. Hence, there is really only one qualitatively distinct bifurcation diagram in this case. The steady state value Q_s in this case is either zero (the homogenous case) or

$$Q_s = -\frac{\sigma_* \epsilon}{c_2(\eta, k_*)} \ . \tag{3.28}$$

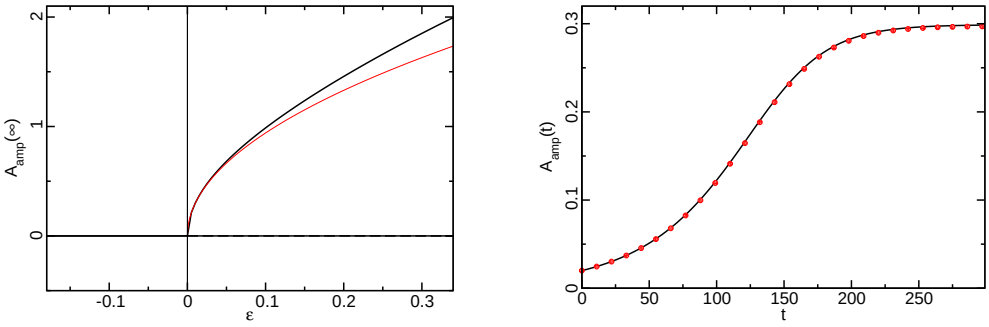

(a) (b)

FIG. 4.1. *1D system with $\eta k_*^2 = 0.4$. In (a) is a bifurcation diagram for the system where dashed lines represent unstable branches and solid lines are stable branches; numerical results are in black and analytic results in red. We find good agreement for smaller ϵ values. In (b) are plots of the numeric (black line) and analytic (red circles) solutions for $A_{amp}(t)$ with $\epsilon = 0.01$ and $Q(0) = 0.01$; there is very good agreement here as well.*

As in the 1-D case, our amplitude equation is only valid to order $|\epsilon|$, so our equation for $A(r,t)$ in this case is simply

$$A(r,t) = \overline{A} + Q(t)J_0(r) \ . \tag{3.29}$$

Note that, since this is a transcritical bifurcation, there is a broken symmetry between positive Q and negative Q solutions, with the former corresponding to a solution that exhibits a bump in A at the origin (hereafter referred to as the "bump solution") and the latter corresponding to a solution that has a ring of high A at the outer edge of the domain (hereafter referred to as the "ring solution"). Our theoretical results from Eq. 3.28 state that the steady state bump solution will exist only for negative ϵ and that it will be unstable, and that the steady state ring solution will exist only for positive ϵ and be stable.

4. Numerical Results. As a verification of our analytical results above, we numerically solve our model system in various geometries. For the dynamical system, we use a fully-implicit Newton-Raphson based solver; for the steady state solutions, we use a Newton-Raphson based relaxation method. For each case, we look at a quantity we will refer to as simply the "amplitude" of A, which will be defined slightly differently in the various geometries.

4.1. 1D. In this geometry, we define the amplitude to be

$$A_{\text{amp}}(t) = \frac{1}{2}\left[A(0,t) - A(\pi,t)\right] \ . \tag{4.1}$$

Since our solution should be 2π periodic, we use the above measure to test the solutions obtained at two points along the phase space. In our experience, the value of the analytical solution at $x = 0$ is often very close to the actual numerical result there, but the analytic and numerical results will start to diverge at $x = \pi$ for higher ϵ values, which is why we choose the measure above. Furthermore, all numerical results in this geometry will use $L = \pi/k_*$ and Neumann boundary conditions.

The first case we explore is a supercritical system, in which $\eta k_*^2 = 0.4$ ($\eta = 0.01$ and $k_* = 2$). The two plots in Fig. 4.1 summarize the results here. Figure 4.1(a)

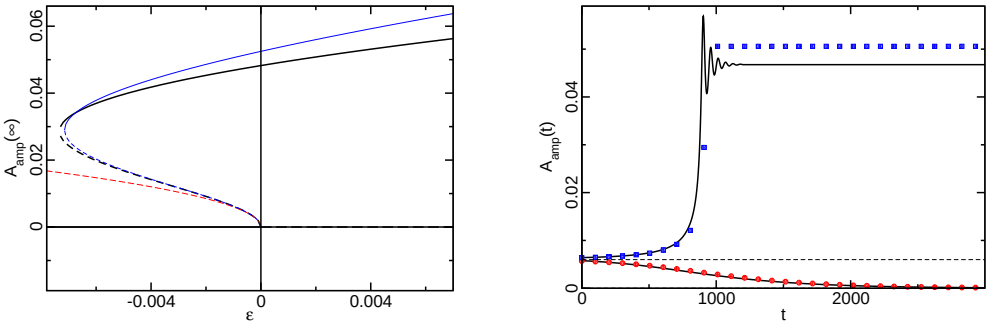

FIG. 4.2. *1D system with $\eta k_*^2 = 0.1$. In (a) is a bifurcation diagram for the system where dashed lines represent unstable branches and solid lines are stable branches; numerical results are in black, analytic results from Eq. 3.20 in red, and a higher order analytic solution in blue. There is good agreement between the numerics and both analytic solutions for smaller ϵ values, but only the higher order analytic solution reproduces the large amplitude branch seen in the numerics. In (b) are plots of the numeric (black lines) and analytic (circles and squares) solutions for $A_{amp}(t)$ with $\epsilon = -0.001$ and varying $Q(0)$; the dashed line represents the analytic steady state value for this ϵ. The lower line corresponds to $Q(0) = 0.0028$, with the analytic solution from Eq. 3.20 in red circles; there is good agreement here between the two. The upper line corresponds to $Q(0) = 0.0032$, with the higher order analytic solution in blue squares. The agreement between these two is reasonable, though the analytic solution predicts a higher steady state value than the numerics.*

shows a bifurcation diagram for our system as derived by computing the steady state value $A_{\rm amp}(\infty)$ as a function of ϵ, plotting both the analytical and numerical results. We find there is good agreement in this case for smaller ϵ values, as predicted. Figure 4.1(b) plots the analytic and numerical solutions for $A_{\rm amp}(t)$ using $\epsilon = 0.01$ and $Q(0) = 0.01$; there is very good agreement here, as this ϵ value is rather small.

The next case we explore is a subcritical system, in which $\eta k_*^2 = 0.1$ ($\eta = 0.01$ and $k_* = 1$), with the results shown in Fig. 4.2. Referring to Fig. 4.2(a), the numerical solutions (black) display the small amplitude, unstable branch predicted by the theory above, and the numerics match the theory (red) well at small ϵ. However, there is also a stable, large amplitude branch in the bifurcation diagram that is not predicted by the theory above. As alluded to before, though, we can continue our analytic solution to the next higher order in ϵ and obtain a much more accurate analytic result that does predict this large amplitude stable branch (blue). We omit the extreme details here, but the general form of this higher order amplitude equation for this example is

$$Q_t = \sigma_*\epsilon\left[1+\epsilon a_1(\eta,k_*)\right]Q + |C_1(\eta,k_*)|\left[1+\epsilon a_2(\eta,k_*)\right]|Q|^2Q - C_2(\eta,k_*)|Q|^4Q\ , \quad (4.2)$$

where a_1, a_2, and C_2 are the new corrections that arise as we move to the higher order. Fig. 4.2(b) shows the evolution of $A_{\rm amp}(t)$ using $\epsilon = -0.001$ and two different values for $Q(0)$. The first value is $Q(0) = 0.0028$, which is just slightly below the unstable branch, so we expect our analytic results above (red) to be close to the numerical results (black), and they are. However, the second $Q(0)$ is 0.0032, which is slightly above the unstable branch, so our results above cannot be used. Instead, we compare with the next higher order analytic result (blue), and find relatively good agreement.

4.2. 2D, radially symmetric. In this geometry, we define the amplitude to be

$$A_{\rm amp}(t) = \frac{1}{2}\left[A(0,t) - A(\alpha_{1,1},t)\right]\ , \quad (4.3)$$

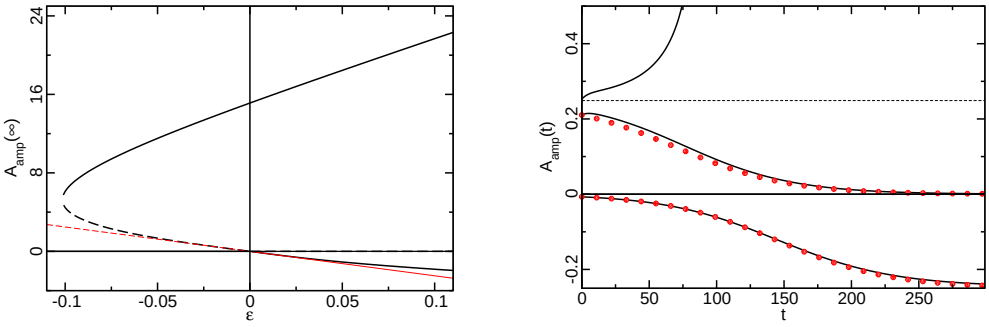

(a) (b)

FIG. 4.3. *Radially symmetric 2D system with $\eta k_*^2 = 0.2$. In (a) is a bifurcation diagram for the system where dashed lines represent unstable branches and solid lines are stable branches; numerical results are in black and analytic results in red. We find good agreement between the two for smaller ϵ values, though the numerics display a large amplitude stable branch that the analytic solution does not. In (b) are plots of the numeric (black lines) and analytic (red circles) solutions for $A_{amp}(t)$ with $|\epsilon| = 0.01$ and varying $Q(0)$. The horizontal dashed line indicates the analytical unstable steady state for $\epsilon < 0$. The lower line corresponds to $Q(0) = -0.01$, $\epsilon > 0$ and the middle line corresponds to $Q(0) = 0.3$, $\epsilon < 0$; the agreement is good in these two cases. The upper line corresponds to $Q(0) = 0.36$, $\epsilon < 0$. This is above the unstable branch, so it grows to the large amplitude stable branch, which is not available from our analytical results.*

for reasons similar to the 1-D definition above. Here, we use $R = \alpha_{1,1}/k_*$ with Neumann boundary conditions, and we choose $\eta k_*^2 = 0.2$ ($\eta = 0.01$ and $k_* = 2\sqrt{5}$). The results are shown in Fig. 4.3. In Fig. 4.3(a), we see our bifurcation diagram for this geometry, which exhibits a transcritical bifurcation near the origin (black) that matches the theory (red) well. However, the numerics also display a large amplitude stable bump solution that our above theory cannot predict. Unlike the subcritical 1-D case above, we do not extend to higher order approximations here. This large amplitude branch indicates that both the bump and ring steady state solutions are stable and available at positive ϵ values, with the bump also being available in both a stable and unstable form over some range of negative ϵ values. Fig. 4.3(b) shows the evolution of both the numeric (black) and analytic (red) $A_{\text{amp}}(t)$ using $|\epsilon| = 0.01$ and three different values for $Q(0)$. The first and lowest value is a ring with $Q(0) = -0.01$ (and positive ϵ), which compares well with the analytic results. The second, intermediate value is a bump with $Q(0) = 0.3$ (and negative ϵ), which is just slightly below the unstable branch, so we expect our analytic result above to work reasonably well in this case, and it does. However, the final value is a bump with $Q(0) = 0.036$ (and negative ϵ), which is slightly above the unstable branch, so our analytic results above cannot be used. Numerically, though, we see that the solution grows until it reaches the stable, large amplitude branch.

4.3. 2-D, non-radially symmetric. In this case, we model the fully 2-D versions of Eqns. 3.7 and 3.8, using the method described previously in [30]. We are mostly concerned in comparing this case to the radially symmetric one above, in terms of the existence of subcritical hotspots with large amplitudes. Another point of comparison will be the existence of the ring solution, which we can predict will not be stable in the non-radially-symmetric case, but will instead break up into separate bump-type solutions.

For the numerics, we use a 128x128 square grid with sides of length $L = 4\alpha_{1,1}/k_*$

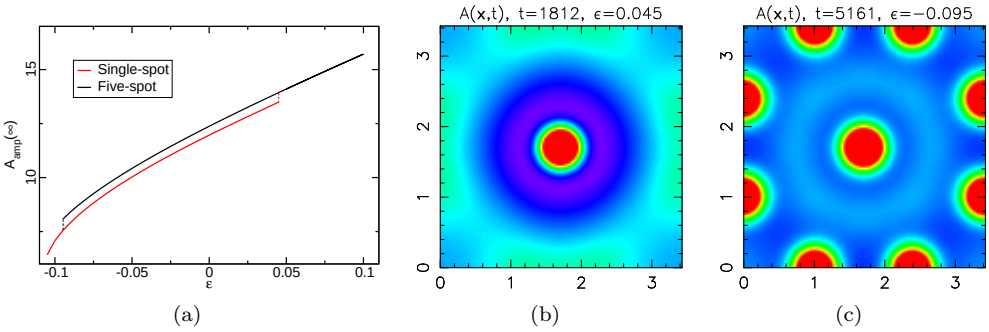

FIG. 4.4. *Full 2D system with $\eta k_*^2 = 0.2$. The colormaps display high A in red, $\overline{A}$ in green, and low A in blue to purple. Shown in (a) is a partial bifurcation diagram for the system, illustrating the possibility of multiple subcritical steady states with varying numbers of hotspots. For $\epsilon < 0$, our initial conditions always lead to a single-spot solution, but it is possible to maintain this single spot even for some positive ϵ values, as shown in (b). At high enough ϵ, the single spot solution gives way to a five-spot solution, which can persist for some range of negative ϵ values, as shown in (c).*

and periodic boundary conditions, with $\eta k_*^2 = 0.2$ ($\eta = 0.01$ and $k_* = 2\sqrt{5}$) as used in the radially symmetric case above. For initial conditions, we start all of the gridpoints at the homogeneous steady state values $\overline{A}$ and $\overline{\rho}$ except for the very center point, which starts with a large excitation of $A = 1000\overline{A}$; this is to ensure that a hotspot develops directly in the center of the domain even if the system is somewhat subcritical. Because of the domain size used and the boundary conditions employed, there are potentially many steady states possible for this system at a given ϵ, and the number of hotspots displayed in each can vary significantly. However, as we are mainly interested in the subcritical case, we will focus on steady states found in this regime. Figure 4.4 displays some of these states. We find that, for these parameters, the minimum ϵ for which a single subcritical spot can develop is around $\epsilon \simeq -0.105$, and that systems with negative ϵ greater than this always develop just one central spot for these initial conditions. If we take one of these single-spot states and slowly increase ϵ above zero, we find that a single spot will remain (Fig. 4.4(b)) until a critical value of ϵ (0.05) is reached, at which point the areas of somewhat elevated A near the edges of the domain break up into separate spots, creating a five-spot solution. Starting with this five-spot solution and slowly decreasing ϵ, on the other hand, shows that this solution persists for negative ϵ that are greater than -0.1 (Fig. 4.4(c)), at which point the outer spots die away, leaving only the center spot remaining.

5. Hotspot suppression. Now that we know our system may exhibit two qualitatively different types of crime hotspots (supercritical and subcritical) it is natural to question what differences may exist, if any, between the behavior of these two classes of pattern with regards to hotspot suppression. As mentioned in the introduction, "hotspot policing" is a law-enforcement strategy whereby more police resources are focused on areas currently believed to be within a hotspot in an effort to disrupt and destroy said hotspot. Studies conducted to test the effectiveness of this strategy reveal that in some instances the hotspots seem to be destroyed, while in others they seem to simply be displaced. The 2D analyses we have performed above seem to offer an explanation as to why these two very different responses to suppression occur (refer to Fig. 4.3). First, imagine a crime hotspot that exists within a linearly stable parameter regime ($\epsilon < 0$); the hotspot is therefore subcritical. If the police presence is

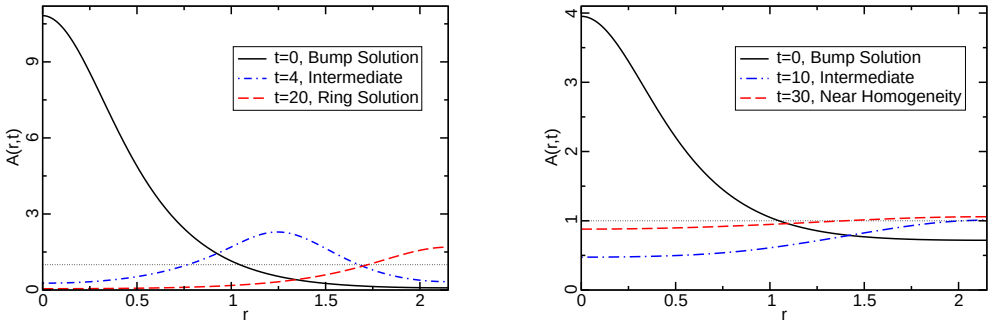

(a) (b)

FIG. 5.1. *Suppression in the radially symmetric 2D system with* $\eta k_*^2 = 0.316$, $\kappa = 3$. *The curves show* $A(r,t)$ *as it evolves following the suppression that occurs at* $t = 0$, *and the horizontal dashed line represents* $A_{cutoff} = 1$. *Shown in (a) is the case* $\epsilon = 0.4$ *and the suppression of the bump drives the system to the ring solution, which persists after suppression is removed. Shown in (b) is the case* $\epsilon = -0.02$ *and the suppression of the bump drives the system to a temporary ring structure that decays to homogeneity once suppression is removed.*

enough to drive the attractiveness of the hotspot below the critical unstable branch of the bump solution in the bifurcation diagram, the system will tend to naturally drop down to the homogeneous state once suppression is relaxed, destroying the hotspot in question utterly. However, imagine now that the hotspot in question exists within the linearly unstable regime ($\epsilon > 0$), and is therefore supercritical. Any effort to suppress the bump solution will simply lead to the attractiveness being displaced to the surrounding area, i.e., the stable ring solution, which will persist after the relaxation of suppression. Of course, in a non-radially symmetric 2D system, the ring solution will not be stable, and will be susceptible to break-up into separate spots. In this case, then, the hotspot policing will have simply lead to a displacement of the hotspot to nearby areas, rather than its destruction.

The above hypothetical scenarios have been verified in computer simulations of the radially symmetric 2D continuous system and the full 2D system in both the continuous and the discrete crime models. To do so, we choose a combination of parameters that are known to be either unstable or stable, whichever is desired. Then, we run simulations as described above in Sec.4 with initial conditions set to initially give a bump solution at the origin (considered to be the center of the field in the full 2D case). We allow the simulation to run until a time t_s when it seems to have reached a steady state, at which point we begin the suppression. This is accomplished by first defining an instantaneous damping field $d(\mathbf{x})$ in the following way

$$d(\mathbf{x}) = \frac{1}{2}\left[1 - \tanh\left[\kappa\left(A(\mathbf{x}, t_s) - A_{\text{cutoff}}\right)\right]\right] \ , \tag{5.1}$$

where κ sets the width of the transition region between total suppression and no suppression and A_{cutoff} sets the attractiveness value above which suppression is desired. This damping field is meant to represent police presence, which is concentrated almost exclusively in the areas of high attractiveness (hotspots). We assume that this presence has two effects. First, the damping field will reduce the crime rate in areas where there is a large police presence ($d \simeq 1$). Second, the police presence will prevent burglars from beginning their search in these same areas. Mathematically, then, our

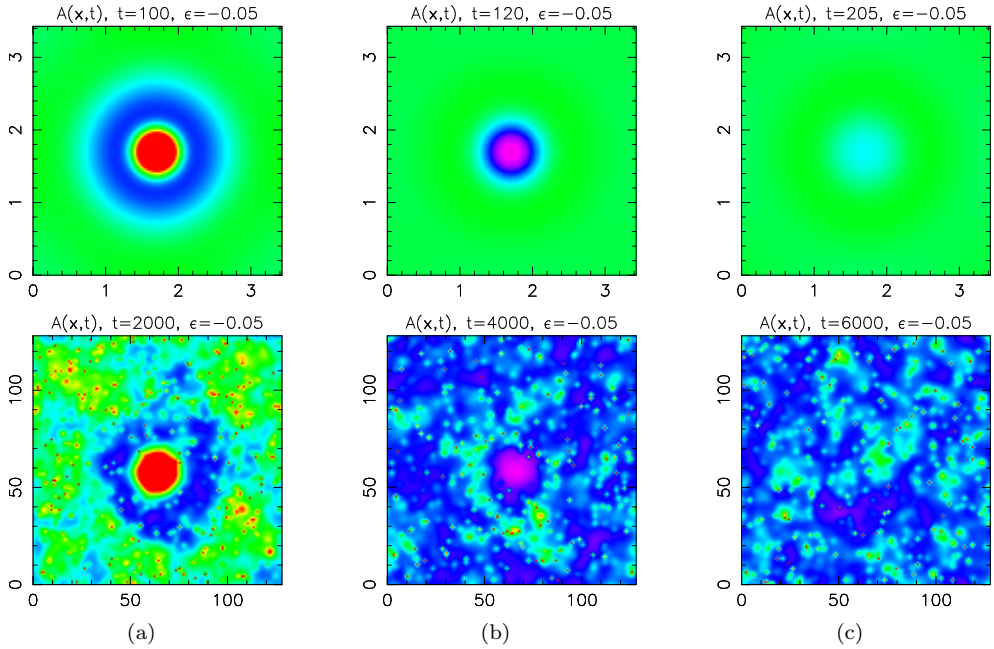

FIG. 5.2. *Suppression results for the full 2D system with* $\eta k_*^2 = 0.2$, $\epsilon = -0.05$, $\kappa = 5$, *and* $A_{cutoff} = 5.72$. *The top row are results from the PDE system, while the bottow row are results from the discrete system with equivalent parameters. These colormaps display high A in red,* $\overline{A}$ *in green, and low A in blue to purple. Shown in (a) is the system configuration right before suppresssion is first implemented. Soon after implementation, the central hotspot has disappeared entirely, but no further spots have emerged (b). Eventually the suppression is lifted and the system begins to adopt the homogenous steady state (c).*

PDE system is modified to

$$\frac{\partial A}{\partial t} = \eta \nabla^2 A - A + A^0 + d\rho A \ , \tag{5.2}$$

$$\frac{\partial \rho}{\partial t} = \vec{\nabla}\left[\vec{\nabla}\rho - \frac{2\rho}{A}\vec{\nabla}A\right] - d\rho A + d\left(\overline{A} - A^0\right) \ . \tag{5.3}$$

Note that this damping field remains unchanged between any two successive t_s values. In other words, the police may remain within an area for some time even after the crime there has been reduced. This is reasonable in the sense that in the real world, police do not have instantaneous information about what areas are most attractive, and must instead rely on where events have occurred in the recent past when deciding where to allocate resources. Therefore, there is an inherent lag between the information possessed by the criminals and that possessed by the police. The typical timescale for this lag in the real world may be on the order of weeks to months [22], which is enough time for new hotspots to emerge [28, 5].

Results for the radially symmetric case are shown in Fig. 5.1, and the hypothetical scenarios play out as anticipated. In the supercritical case, suppression of the bump drives the system to the ring solution, which, due to its stability, remains after suppression is relaxed (Fig. 5.1(a)). Suppression of the subcritical bump initially sends the system to a ring-like state as well, since the suppression by definition will cause the origin to have very low A values, leaving the outer edge as the only place

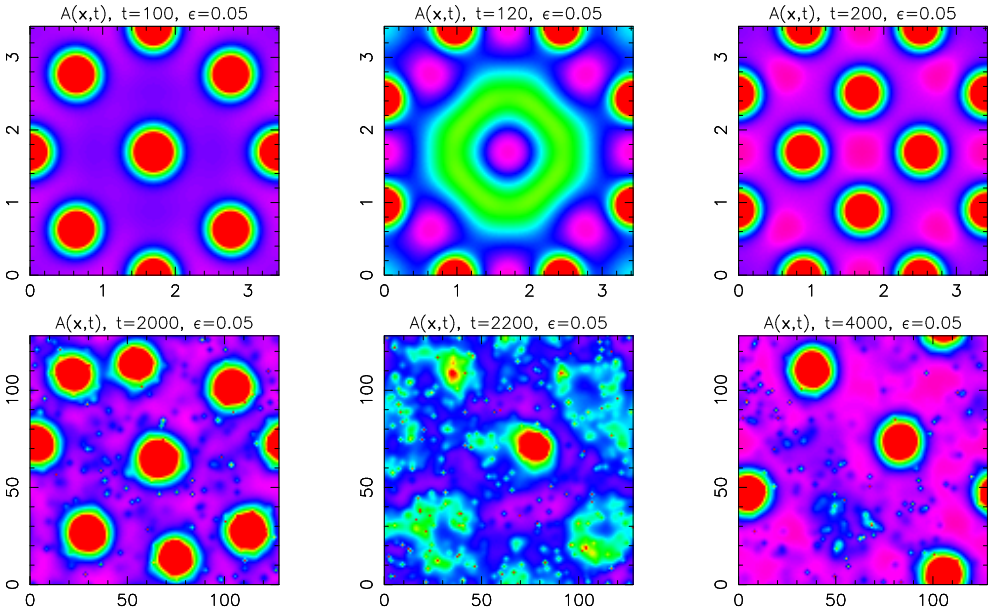

FIG. 5.3. *Suppression results for the full 2D system with* $\eta k_*^2 = 0.2$, $\epsilon = 0.05$, $\kappa = 5$, *and* $A_{cutoff} = 6.12$. *The top row are results from the PDE system, while the bottow row are results from the discrete system with equivalent parameters. These colormaps display high A in red,* $\overline{A}$ *in green, and low A in blue to purple. Before suppression is first implemented, the system displays a number of hotspots (a). Soon after the implementation of suppression the original hotspots vanish, but the attractiveness of the neighboring regions correspondingly increases, leading to a transient structure resembling the ring solution that surrounds the location of the original central hotspot (b). By the time the next suppression time* T_s *has arrived, a new steady state featuring hotspots near the original ones has been achieved (c).*

for criminal activity to occur. However, once the suppression is removed, the ring's instability causes it to decay to the homogeneous state, and the original hotspot is now destroyed (Fig. 5.1(b)).

Figure 5.2 illustrates the effects of hotspot suppression in a fully 2D, subcritical system. Before suppression (Fig. 5.2(a)), we see that our initial condition has lead to a stable hotspot in the center of the field in both the continuum and discrete cases, though the discrete case also displays some quasi-hotspots near the edges of the domain due to random fluctuations that push the system at least temporarily above the unstable branch . Once suppression is introduced (Fig. 5.2(b)), the hotspot dies away rather quickly, leaving an area of very low A in the center where the police presence remains and a faint ring near the domain edges. Critically, though, we do not see the emergence of new hotspots. Finally, when the next T_s is reached (Fig. 5.2(c)), there is actually no suppression needed since no hotspots remain, and the "coldspot" in the center returns to the homogeneous value soon after the police leave the area. As predicted, the suppression was effective in eradicating the hotspot in the subcritical case.

Figure 5.3 illustrates the effects of hotspot suppression in a fully 2D, supercritical system. Before suppression (Fig. 5.3(a)), we see that our initial condition has lead not only to a hotspot in the center of the field, but a number of other hotspots have

developed near the edge due to the linear instability of the system. Once suppression is introduced (Fig. 5.3(b)), the original hotspots disappear quickly. However, we see in the continuum case especially that the eradication of these spots has simply pushed the system into a different non-homogeneous configuration, with a temporary structure resembling the ring solution surrounding the area where the central hotspot was located. Finally, by the time the next T_s has arrived (Fig. 5.3(c)), the system has reached a new steady state that exhibits hotspots in areas near where the original spots were. So, the suppression was ineffective in eradicating the supercritical hotspots, and merely lead to their displacement.

6. Conclusions. Through a weakly nonlinear analysis of our coupled PDE system (Eqns. 2.1 and 2.2), we have shown that in both the 1D and 2D cases, our system may exhibit stable hotspots in both the supercritical and subcritical regime. The existence of the subcritical hotspots offers another mechanism for crime pattern formation, in addition to the linear instability discussed in our previous work.

Importantly, these distinct hotspot mechanisms may help explain the varying measures of success that police agencies have when attempting to suppress hotspots. In the supercritical case, suppression of a hotspot seems to simply displace the spot to neighboring regions, as the bump solution gives way to the ring solution, which will either be a new stable state (in the radially symmetric case) or will then break up into separate bumps (in the non-radially symmetric case); this is illustrated in Figs. 5.1(a) and 5.3. In the subcritical case, on the other hand, the suppression of the hotspot below the unstable bump solution branch of the bifurcation diagram (Fig. 4.3) should destroy it completely, as the ring solution is unstable in this regime and will decay to the homogeneous state once supression is removed; this is illustrated in Figs. 5.1(b) and 5.2.

As a corollary to this argument, we point out that the existence of these large amplitude branches introduces the possibility of hysteresis into the system. That is, if the parameters of the system are slowly varying with time (as social or economic conditions vary, perhaps), what was once a peaceful city may experience a sudden burst of crime once the stability threshold is passed, rather than the crime slowly increasing as the parameters move further into the unstable regime. In this situation, police attempts at suppression may only have the effect of displacing crime hotspots. Furthermore, if the parameters then begin to decrease, this high level of crime may persist until things are even better than when the initial outbreak occurred, though once the stability threshold is passed police suppression should help in destroying hotspots.

Acknowledgments. The authors would like to thank George Tita, Lincoln Chayes, Paul Jones, and the Los Angeles Police Department for helpful discussions. This work was supported by NSF grant BCS-0527388, ARO MURI grant 50363-MA-MUR, and the Department of Defense.

REFERENCES

[1] L. Anselin, J. Cohen, D. Cook, W. Gorr, and G. Tita, *Spatial analyses of crime*, in Criminal Justice 2000, D. Duffee, ed., vol. 4, National Institute of Justice, Washington, D.C., 2000, pp. 213–262.

[2] M.D. Betterton, *Theory of structure formation in snowfields motivated by penitentes, suncups, and dirt cones*, Physical Review E, 63 (2001).

[3] K.J. Bowers and S.D. Johnson, *The Role of Publicity in Crime Prevention: Findings from the Reducing Burglary Initiative*, Home Office, London, 2003.

[4] A.A. Braga, *The effects of hot spots policing on crime*, Annals of the American Academy of Political and Social Science, 578 (2001), pp. 104–125.
[5] ———, *The crime prevention value of hot spots policing*, Psicothema, 18 (2006), pp. 630–637.
[6] A.A. Braga, D.L. Weisburd, E.J. Waring, L. Green-Mazerolle, W. Spelman, and F. Gajaewski, *Problem-oriented policing in violent places: A randomized controlled experiment*, Criminology, 37 (1999), pp. 541–580.
[7] P.J. Brantingham and P.L. Brantingham, *Anticipating the displacement of crime using the principles of environmental criminology*, Crime Prevention Studies, 16 (2003), pp. 119–148.
[8] M. Burger, M. Di Francesco, and Y. Dolak-Struss, *The Keller-Segel model for chemotaxis with prevention of overcrowding: Linear vs. nonlinear diffusion*, SIAM Journal on Mathematical Analysis, 38 (2006), pp. 1288–1315 (electronic).
[9] H.M. Byrne and M.R. Owen, *A new interpretation of the Keller-Segel model based on multiphase modelling*, Journal of Mathematical Biology, 49 (2004), pp. 604–626.
[10] P.Y. Chan and N. Goldenfeld, *Steady states and linear stability analysis of precipitation pattern formation at geothermal hot springs*, Physical Review E, 76 (2007).
[11] M.C. Cross and P.C. Hohenberg, *Pattern formation outside of equilibrium*, Reviews of Modern Physics, 65 (1993), pp. 851–1112.
[12] M. del Pino and J. Wei, *Collapsing steady states of the Keller-Segel system*, Nonlinearity, 19 (2006), pp. 661–684.
[13] J.M. Epstein and R.L. Axtell, *Growing Artificial Societies: Social Sciences from the Bottom Up*, The Brookings Institution, Washington, D.C., 1996.
[14] C. Escudero, *The fractional Keller-Segel model*, Nonlinearity, 19 (2006), pp. 2909–2918.
[15] M.A. Herrero and J.J.L. Velázquez, *Chemotactic collapse for the Keller-Segel model*, Journal of Mathematical Biology, 35 (1996), pp. 177–194.
[16] S.D. Johnson and K.J. Bowers, *The burglary as clue to the future: The beginnings of prospective hot-spotting*, European Journal of Criminology, 1 (2004), pp. 237–255.
[17] ———, *Domestic burglary repeats and space-time clusters: The dimensions of risk*, European Journal of Criminology, 2 (2005).
[18] S.D. Johnson, K.J. Bowers, and A. Hirschfield, *New insights into the spatial and temporal distribution of repeat victimisation*, The British Journal of Criminology, 37 (1997).
[19] E.F. Keller and L.A. Segel, *Initiation of slime mold aggregation viewed as an instability*, Journal of Theoretical Biology, 26 (1970), pp. 399–415.
[20] G.L. Kelling, *The Kansas City Preventative Patrol Experiment: A Technical Report*, Police Foundation, Kansas City, MO, 1974.
[21] S. Luckhaus and Y. Sugiyama, *Large time behavior of solutions in super-critical cases to degenerate Keller-Segel systems*, M2AN. Mathematical Modelling and Numerical Analysis, 40 (2006), pp. 597–621.
[22] M.H. Moore and A.A. Braga, *Measuring and improving police performance: The lessons of compstat and its progeny*, Policing: An International Journal of Police Strategies & Management, 26 (2003), pp. 439–453.
[23] S.V. Petrovskii and H. Malchow, *A minimal model of pattern formation in a prey-predator system*, Mathematical and Computer Modelling, 29 (1999), pp. 49–63.
[24] T. Reichenbach, M. Mobilia, and E. Frey, *Mobility promotes and jeopardizes biodiversity in rock-paper-scissors games*, Nature, 448 (2007), pp. 1046–1049.
[25] T.A. Reppetto, *Crime prevention and displacement phenomenon*, Crime & Delinquency, 22 (1976), pp. 166–167.
[26] T.C. Schelling, *Dynamic models of segregation*, Journal of Mathematical Sociology, 1 (1971), pp. 143–186.
[27] T. Senba, *Type II blowup of solutions to a simplified Keller-Segel system in two dimensional domains*, Nonlinear Analysis. Theory, Methods & Applications. An International Multidisciplinary Journal. Series A: Theory and Methods, 66 (2007), pp. 1817–1839.
[28] L. Sherman and D. Rogan, *Deterrent effects of police raids on crack houses: A randomized controlled experiment*, Justice Quarterly, 12 (2006), pp. 755–782.
[29] M.B. Short, J.C. Baygents, J.W. Beck, D.A. Stone, R.S. Toomey, and R.E. Goldstein, *Stalactite growth as a free-boundary problem: A geometric law and its platonic ideal*, Physical Review Letters, 94 (2005).
[30] M.B. Short, M.R. D'Orsogna, V. Pasour, J. Brantingham, G. Tita, A. Bertozzi, and L. Chayes, *A statistical model of criminal behavior*, Mathematical Models and Methods in Applied Sciences, 18 (2008), pp. 1249–1267.
[31] Y. Sugiyama, *Global existence in sub-critical cases and finite time blow-up in super-critical cases to degenerate Keller-Segel systems*, Differential and Integral Equations. An International Journal for Theory & Applications, 19 (2006), pp. 841–876.

[32] A.M. Turing, *The chemical basis of morphogenesis*, Philosophical Transactions of the Royal Society of London Series B-Biological Sciences, 237 (1952), pp. 37–72.

[33] M. van Hecke, P.C. Hohenberg, and W. van Saarloos, *Amplitude equations for pattern forming systems*, in Fundamental Problems in Statistical Mechanics, H. van Beijeren and M.H. Ernst, eds., vol. VIII, North-Holland, Amsterdam, 1994, pp. 245–278.

[34] J.J.L. Velázquez, *Well-posedness of a model of point dynamics for a limit of the Keller-Segel system*, Journal of Differential Equations, 206 (2004), pp. 315–352.

[35] D. Weisburd and J.E. Eck, *What can police do to reduce crime, disorder, and fear?*, Annals of the American Academy of Political and Social Science, 593 (2004), pp. 42–65.

[36] D. Weisburd, L.A. Wyckoff, J. Ready, J.E. Eck, J.C. Hinkle, and F. Gajewski, *Does crime just move around the corner? A controlled study of spatial displacement and diffusion of crime control benefits*, Criminology, 44 (2006), pp. 549–592.